

Characterization of Linear Electromagnetic Observables in Stochastic Field-to-Wire Couplings

Ousmane O. Sy^{1, 3, *}, Martijn C. van Beurden¹, and Bastiaan L. Michielsen²

Abstract—This article presents a method to characterize stochastic observables defined by induced surface currents and fields in electromagnetic interactions with uncertain configurations. As the covariance operators of the stochastic distributions and fields are not compact, a strict Karhunen-Loève (KL) approach is not possible. Instead, we apply a point-spectrum regularization by expanding the stochastic quantities on a finite-element-like basis. The coefficients of the KL expansion are approximated analytically in a polynomial-chaos (PC) expansion. The novelty of our approach resides in its ability to handle multiple PC expansions simultaneously and determine the *orders* of the KL and PC expansions *adaptively*. This method is illustrated through the example of the voltage induced at the port of a random thin-wire frame illuminated by random plane waves. The results show the accuracy and computational efficiency of the proposed method, which provides a complete characterization of the randomness of the observable.

1. INTRODUCTION

Electronic systems have to properly function in a vast range of operational scenarios. For example, electronic systems have different compositions due to customer wishes and upgrades over time. This generates many uncertainties in the operational conditions of the system. Other types of uncertainties that occur are ageing and drift, production tolerances, and locations of cable trees due to individual decisions taken by an installer of a system. Under all such conditions, which are partly outside the control of the manufacturer, the manufacturer has to guarantee safe and proper functioning, as well as EMC compliance of the system. Since the number of potential scenarios and deviations from the ideal system is vast, it is rapidly becoming unpractical or impossible to guarantee the proper functioning of a system based on a limited set of deterministic simulations and well-controlled experiments that are induced by practical time and budget constraints.

Research in stochastic electromagnetic fields approaches this dilemma from a different perspective. By introducing uncertainties in a setup from the start, one aims at generating a sufficiently rich stochastic ensemble that will properly represent the entire range of device variations and operational conditions [1, 2]. This rationale has been adopted in reverberation-chamber measurements, where a rich set of electromagnetic fields impinges upon a device under test [3, 4]. A similar train of thoughts can be observed in the construction of numerical methods for CAD tools [5].

Popular methods to analyze stochastic systems are the Monte-Carlo method and Stochastic Collocation, both of which use an underlying parameterized deterministic model and a sampling scheme guided by the assumptions on the probability density functions of the parameters [6–9]. The advantage is that the deterministic model is tackled with well-established numerical methods and that this model

Received 30 June 2016, Accepted 2 October 2016, Scheduled 14 October 2016

* Corresponding author: Ousmane Oumar Sy (ousmane.o.sy@jpl.nasa.gov).

¹ Department of Electrical Engineering, Eindhoven University of Technology, Den Dolech 2, 5600 MB, Eindhoven, The Netherlands.
² ONERA — DEMR, BP 74025, 2, av. Edouard Belin, 31055 Toulouse Cedex 4, France. ³ Now at Jet Propulsion Laboratory, California Institute of Technology, Pasadena, California, USA.

can be treated as a black box that produces responses for the sampled parameters. Nevertheless, a single model evaluation can already be time-consuming and a sampling approach readily requires several hundreds or thousands of evaluations. Therefore, economizing on the number of model evaluations is an important aspect in constructing numerical tools for stochastic problems.

In the present paper, we address electromagnetic-scattering problems with stochastic parameters in both configuration and excitation field. As in previous papers, the Lorentz reciprocity theorem allows us to compute an observable, e.g., an induced voltage, for multiple excitation fields by solving a linear system for a single right-hand side per variation in the configuration [10, 11]. To allow for the computation of an observable for stochastic excitations and simultaneously avoid the construction of extensive libraries of numerical solutions, we exploit a Karhunen-Loève (KL) decomposition of the essential stochastic distributions and fields [12, 13]. To ensure that the KL expansion can be derived, i.e., that the covariance operators of the fields and currents are compact, the stochastic processes are expanded on finite-element basis functions. The KL decomposition provides a method for determining the degrees of freedom in the problem while a polynomial-chaos (PC) expansion leads to a rapidly converging approximation of the observables as functions on the probability space [14, 15]. We apply the PC expansion *semi-intrusively*, i.e., instead of applying the PC expansion directly to the induced voltage, we expand the fields and currents that define the voltage, thereby achieving computational gains. By aiming to fully characterize the randomness of the observable, this article extends previous efforts where the semi-intrusive approach was used to determine only the mean and variance of the observable [3, 16].

The general practice is to truncate the KL expansion based on the decay of the eigenvalues of the covariance and use a fixed order for the PC expansion based on its variance. Both choices guarantee the root-mean-square accuracy but not the accuracy of the full distribution. We address these issues by using a higher-order statistic, viz. the Kolmogorov-Smirnov statistic of a canonical voltage, to *jointly and adaptively* determine the *orders of the KL and PC expansions*. The required steps in the recipe are made explicit and we demonstrate that the combination of the techniques results in a versatile and powerful scheme. As such, our algorithm focuses on an adaptive p -refinement of the PC expansion, rather than adaptive h -refinement methods proposed in the multi-element probabilistic collocation method [8], or the hierarchical sparse-grid collocation method [9].

The outline of this article is as follows. Section 2 describes the test case used as a prototype to study linear electromagnetic interactions, i.e., a randomly shaped thin-wire frame connected to a random impedance and illuminated by plane waves. Section 3 presents the stochastic model that is sought and built using Karhunen-Loève and polynomial-chaos spectral expansions. The adaptive scheme devised to ensure the joint convergence of the KL and PC expansions is described in Section 4 and illustrated in Section 5 through the KLPC expansion of the current flowing on the random thin-wire frame. The KLPC model is then used in Section 6 to accurately approximate the probability distribution of the voltage induced at the port of the setup by deterministic or random incident fields. The computational cost of the KLPC approach is discussed in Section 7.

2. STOCHASTIC LINEAR-INTERACTION PROBLEM

This section describes a stochastic linear electromagnetic interaction problem involving a thin-wire setup. Thin-wire structures play an important role in antenna theory and in electromagnetic compatibility (EMC) due to their presence in harnesses and cables that interconnect electronic devices. At high frequencies, these wires even behave as radiating elements that must be accounted for to properly describe the total electromagnetic field.

2.1. Definition of the Interaction Geometry

We consider a generic configuration derived from an EMC benchmark [17] and shown in Fig. 1. The setup, which is considered in free space and in the time-harmonic regime, consists of a perfectly electrically conducting (PEC) thin-wire frame W with a circular cross-section of diameter $a = 1$ mm that is negligible compared to the wavelength λ . One of the ports of W is open (left), whereas the other port (right) is connected to the ground plane via a load $Z = R + j\xi \in \mathcal{Z} \subset [0, \infty) \times \mathbb{R}$.

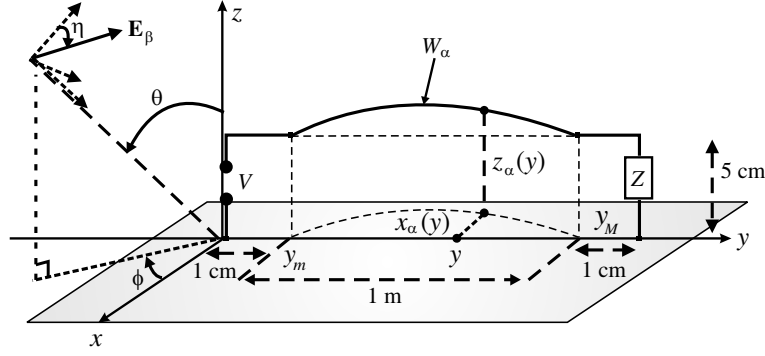


Figure 1. Interaction configuration: perfectly conducting thin-wire frame W_α connected to a load Z and located above a ground plane, incident field \mathbf{E}_β and observable V induced at the port of W_α .

The shape of W results from the geometrical deformation of a reference transmission line W_0 located 5 cm above a PEC ground plane. The axis of W is defined with respect to W_0 through the smooth mapping

$$\tau_\alpha(\mathbf{r}_0) = \mathbf{r}_0 + \begin{cases} (\alpha^x \mathbf{u}_x + \alpha^z \mathbf{u}_z) \sin\left(\pi \frac{y_0 - y_m}{y_M - y_m}\right), & \text{if } y_0 \in [y_m, y_M], \\ \mathbf{0}, & \text{otherwise,} \end{cases} \quad (1)$$

for any $\mathbf{r}_0 = (x_0, y_0, z_0) \in W_0$, with $(\mathbf{u}_x, \mathbf{u}_y, \mathbf{u}_z)$ the Cartesian basis. The geometrical deformations are controlled by the vector $\alpha = (\alpha^x, \alpha^z)$, which belongs to $\mathcal{A} = \mathcal{A}^x \times \mathcal{A}^z$, with $\mathcal{A}^x = \mathcal{A}^z = [-0.03; 0.03]$ m. To mark the dependence of W on α , the deformed wire is written as W_α . The impedance of the wire is $Z = R + j\xi$ with a deterministic resistance $R = 50 \Omega$ and a reactance $\xi \in \mathcal{X} = [-5, 5] \Omega$. Geometrical uncertainties of the setup correspond to an indetermination of α in \mathcal{A} , while material uncertainties translate in an indetermination of ξ in \mathcal{X} . The consequences of these uncertainties can be severe when dealing with a resonant structure such as W_α , as will be shown in Section 2.3.1.

To quantify these uncertainties, a stochastic framework is adopted by gathering the uncertain parameters of the configuration in the vector $\gamma = (\alpha, \xi) \in \mathcal{G} = \mathcal{A} \times \mathcal{X}$ and by regarding the variations of γ in \mathcal{G} as random. Specifically, γ is a random vector, which has mutually statistically independent components and follows the probability distribution $P_{\mathcal{G}}$ that is known *a priori* or derived from the observations of realizations of the system.

2.2. Definition of the Incident Field

The externally generated incident field is denoted \mathcal{E}_β where $\beta \in \mathcal{B} \subset \mathbb{R}^m$ gathers parameters such as the amplitude, polarization and direction of propagation of the field. This field is assumed to have a plane-wave spectrum, denoted \mathbf{E}_β , with

$$\mathcal{E}_\beta : \mathbb{R}^3 \ni \mathbf{r} \mapsto \int_{\mathcal{S}} \mathbf{E}_\beta(\mathbf{k}_i) e^{-j\mathbf{k}_i \cdot \mathbf{r}} d^3\mathbf{k}_i \in \mathbb{C}^3, \quad (2)$$

where $\mathcal{S} = \left\{ \frac{2\pi}{\lambda} \mathbf{u}_i, \text{ with } \mathbf{u}_i \in \mathbb{R}^3, \|\mathbf{u}_i\| = 1 \right\}$ is the set of wavevectors and $\mathbf{E}_\beta(\mathbf{k}_i) \in \mathbb{C}^3$ is the polarization vector, with $\mathbf{E}_\beta(\mathbf{k}_i) \cdot \mathbf{k}_i = 0$, for any $\mathbf{k}_i \in \mathcal{S}$. The support of \mathbf{E}_β in \mathcal{S} defines the directions of incidence (θ_i, ϕ_i) in polar coordinates. For our purposes, the incident fields are assumed to impinge from the directions $(\theta, \phi) \in [0, \pi/2] \times [-\pi/2, \pi/2]$, i.e., $\mathcal{S} = \left\{ (2\pi/\lambda) \mathbf{u}_r(\theta, \phi), \theta \in [0, \pi/2], \phi \in [-\pi/2, \pi/2] \right\}$, with

$$\mathbf{u}_r(\theta, \phi) = -(\sin \theta \cos \phi \mathbf{u}_x + \sin \theta \sin \phi \mathbf{u}_y + \cos \theta \mathbf{u}_z). \quad (3)$$

Uncertainties in \mathbf{E}_β are also handled stochastically by assuming that β is randomly distributed in \mathcal{B} according to a known distribution $P_{\mathcal{B}}$. Since the incident field is generated by sources external to the scatterer, γ and β are assumed mutually statistically independent.

2.3. Induced Voltage as Observable

The voltage V induced at the port of the system by \mathcal{E}_β is defined as

$$V(\gamma, \beta) = - \int_{\partial W_\alpha} \mathcal{J}_\gamma(\mathbf{r}) \cdot \mathcal{E}_\beta(\mathbf{r}) dS(\mathbf{r}) \quad \in \mathbb{C}, \quad (4)$$

where the distribution $\mathcal{J}_\gamma(\mathbf{r})$ depends solely on γ as it is induced on the mantle of W_α in a transmitting state, i.e., by a unit current source applied to the port in the absence of \mathcal{E}_β [11]. To accurately account for the deformation of W_α and the boundary conditions at the load Z , \mathcal{J}_γ is computed by solving the electric-field integral equation (EFIE) associated with the transmitting state. The computation and solution of the EFIE impedance matrix are carried out efficiently using an approximate-kernel Pocklington equation [18] and quadratic-segment basis functions [19]. Hence, \mathcal{J}_γ is a nonlinear function of γ , each evaluation of which incurs a given numerical cost. Alternative electromagnetic models could have been considered, e.g., based on transmission-line theory [20, 21]. However, one must make sure that these models can properly handle the varying height-above-ground of the thin wire.

2.3.1. Motivation of the Uncertainty Quantification

The electromagnetic behavior of the setup is illustrated in Fig. 2 as a function of frequency for a wire connected to a resistance $Z = 50 \Omega$. The incident field is a parallelly polarized plane wave with an electric field of amplitude $1 \text{ V} \cdot \text{m}^{-1}$, propagating along the direction $(\theta = 45^\circ, \phi = -45^\circ)$. This graph shows the amplitude $|V|$ of the induced voltage for the mean configuration $\alpha_{\text{AVG}} = (0, 0)$ and the “extreme” deformations obtained with $\alpha_{\text{MAX}} = [0.03, 0.03] \text{ m}$ and $\alpha_{\text{MIN}} = -\alpha_{\text{MAX}}$. The current \mathcal{J}_γ is computed via a method of moments (MoM) by discretizing the axis of the wire into 224 segments. This produces a uniform mesh with 5 mm long segments.

These plots show resonance peaks in the spectrum of $|V|$. The effects of the deformations are noticeable through the shift between the resonance frequencies of α_{AVG} compared to those of α_{MIN} and α_{MAX} . For instance, at $f_1 = 1997 \text{ MHz}$, if the deformations are ignored, using the response of α_{AVG} for all configurations can lead to an over-estimation of the voltage by up to 4 dB. Hence, the need for

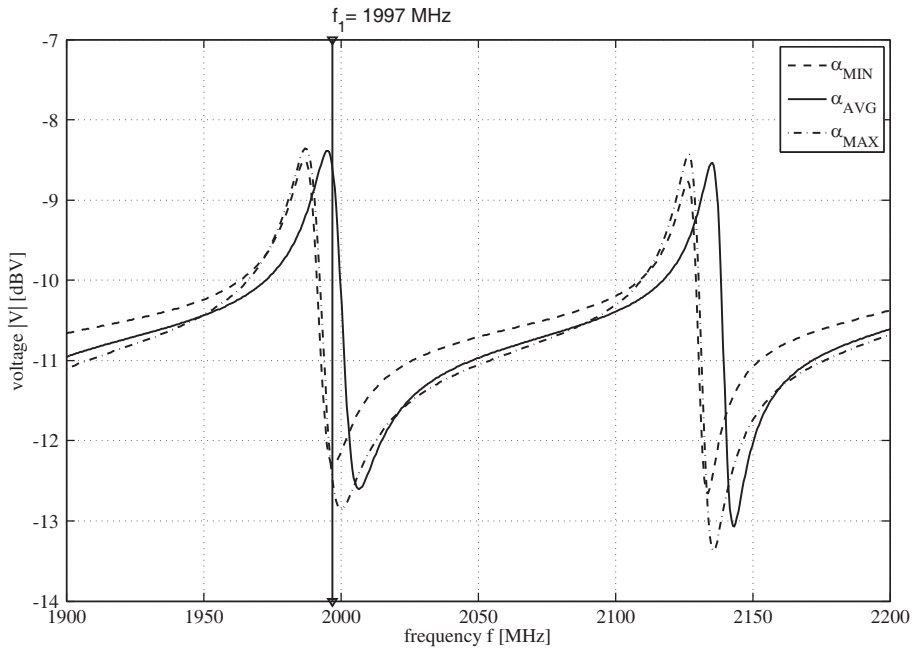


Figure 2. Deterministic voltage induced by a parallelly polarized plane wave at the port of wires connected to a load $Z = 50 \Omega$. The frequency studied in this article is $f_1 = 1997 \text{ MHz}$.

an uncertainty quantification at such a frequency, which is the frequency considered in the remainder of the article.

2.3.2. Stochastic Parametrization of the Voltage

Through Eq. (4), the randomness of γ or β induces the randomness of V . However, unlike γ or β , the probability distribution P_V of V is unknown. The aim of the stochastic approach is to characterize or approximate P_V given P_G , P_B and the dependence of V on (γ, β) . Due to the numerical and nonlinear dependence of V on (γ, β) , P_V cannot be determined analytically.

The distribution P_V can be characterized by a Monte-Carlo (MC) approach, viz. by generating a large set of samples of V using values of (γ, β) drawn randomly according to P_G and P_B . Then, this large dataset can be used to compute statistical moments or approximate the cumulative distribution function (CDF) of V . However, a drawback of this approach is that whenever either P_G or P_B changes, a new MC analysis is required. Second, the generation of a large MC dataset implies the solution of as many boundary-value problems, which rapidly becomes cumbersome numerically.

To circumvent the first limitation, we reformulate the observable to separate the effects of the geometrical uncertainties from the uncertainties due to \mathcal{E}_β . Next, we apply a spectral expansion to express the dependency of V on γ and β explicitly in terms of polynomials, which in turn eases the statistical processing of V significantly.

2.3.3. Spectral Reformulation of the Observable

Although \mathcal{E}_β is independent of the scattering device, it must still be evaluated over the support of \mathcal{J}_γ , viz. at a point on the mantle of the wire $\mathbf{r} \in \partial W_\alpha$, to compute V . Therefore, the geometrical modifications of the setup also affect \mathcal{E}_β , thereby complicating the characterization of the variations of \mathcal{J}_γ independently from \mathcal{E}_β . This difficulty is avoided by using a spectral definition of V through Plancherel's theorem [22, p. 188], i.e.,

$$V(\gamma, \beta) = - \int_{\mathcal{S}} \mathbf{J}_\gamma(\mathbf{k}) \cdot \mathbf{E}_\beta^*(\mathbf{k}) d^3\mathbf{k} \stackrel{\text{def}}{=} - \langle \mathbf{J}_\gamma; \mathbf{E}_\beta \rangle_{\mathcal{S}}, \quad (5)$$

where (*) is the complex conjugation and \mathbf{J}_γ the Fourier transform of \mathcal{J}_γ

$$\mathbf{J}_\gamma : \mathcal{S} \ni \mathbf{k} \longmapsto \int_{\partial W_\alpha} \mathcal{J}_\gamma(\mathbf{r}) e^{-j\mathbf{k}\cdot\mathbf{r}} dS(\mathbf{r}) \in \mathbb{C}^3. \quad (6)$$

The advantage of Eq. (5) over Eq. (4) is that the randomness of the system is now entirely contained in \mathbf{J}_γ and can be quantified by characterizing the randomness of \mathbf{J}_γ only. The resulting information can be re-used to obtain statistics of V , regardless of the type of incident field.

3. STOCHASTIC SEMI-INTRUSIVE KLPC MODEL

3.1. Outline of the Method

In this section, we propose a representation of the stochastic observable to highlight the most efficient way of doing the numerical computations. In the integral representation of Eq. (5), \mathbf{J}_γ is a stochastic field defined by the probability space \mathcal{G} and mapping each $\gamma \in \mathcal{G}$ to the space of infinitely smooth fields with their support in \mathcal{S} , which is denoted $\mathcal{E}(\mathcal{S}, \mathbb{C}^3)$ [22, p.92]. As for \mathbf{E}_β , it is a stochastic generalized function defined by the probability space \mathcal{B} and valued in $\mathcal{E}'(\mathcal{S}, \mathbb{C}^3)$, i.e., the dual space of $\mathcal{E}(\mathcal{S}, \mathbb{C}^3)$. The objective is to have a convenient representation of the objects in the definition of the observable to access the dependency of the observable on the stochastic parameters (γ, β) . This in turn will significantly ease the evaluation of the statistical properties of V .

We suppose that \mathbf{J}_γ has the following approximation

$$\mathbf{J}_\gamma(\mathbf{k}) \approx \sum_{n=0}^N \mathbf{J}_n(\mathbf{k}) \rho_n(\gamma), \quad \forall \gamma \in \mathcal{G}, \quad (7)$$

where $\{\mathbf{J}_n\}_{n=0,\dots,N}$ is a set of deterministic vector fields regular in \mathcal{S} and $\{\rho_n\}_{n=0,\dots,N}$ is a set of orthogonal functions defined on \mathcal{G} and which will be approximated via polynomials. This approximation, which will be obtained by applying Karhunen-Loève (KL) and polynomial-chaos (PC) expansions described in the next section, yields a model that is henceforth denoted KLPC. Inserting Eq. (7) in (5) leads to

$$V(\gamma, \beta) \approx \sum_{n=0}^N \rho_n(\gamma) \nu_n(\beta), \quad \text{with } \nu_n(\beta) = -\langle \mathbf{J}_n; \mathbf{E}_\beta \rangle_{\mathcal{S}}. \quad (8)$$

Equation (8) is already an advantageous representation of the observable when \mathbf{E}_β is cheap to compute, e.g., when it consists of the sum of a small number of plane waves. Indeed, since $\{\mathbf{J}_n\}_{n=0,\dots,N}$ are deterministic, they need to be computed only once and statistical operations only involve the polynomials that approximate $\{\rho_n(\gamma)\}_{n=0,\dots,N}$, which are easy to evaluate. This way of applying the PC expansion is semi-intrusive, i.e., intrusive with respect to the final observable that is V , and non-intrusive for \mathbf{J}_γ and \mathbf{E}_β as the PC expansion is not applied to the operators that define these two quantities.

3.2. Stochastic Spectral Model: KLPC Expansion

Without loss of generality, the KLPC expansion is described for \mathbf{J}_γ . Since the covariance of \mathbf{J}_γ is not necessarily compact, a Karhunen-Loève decomposition cannot be applied *stricto sensu*. To sidestep this issue, a weak formulation is used by expanding the stochastic processes on a set of deterministic finite-element basis functions, which is denoted $\mathcal{H} = \{h_\ell : \mathcal{S} \rightarrow \mathbb{R}\}_{\ell=1,\dots,N_S}$ and may consist, e.g., of pulses or triangular functions. Expanding all the components of \mathbf{J}_γ in terms of these functions leads to

$$\mathbf{J}_\gamma(\mathbf{k}) \approx \sum_{\ell=1}^{N_S} \mathbf{I}_\gamma(\ell) h_\ell(\mathbf{k}), \quad (9)$$

$$\text{where } \mathbf{I}_\gamma(\ell) = \langle \overline{h_\ell}; \mathbf{J}_\gamma \rangle_{\mathcal{S}} \in \mathbb{C}^3, \quad \forall \ell = 1, \dots, N_S, \quad (10)$$

with $\{\overline{h_\ell}\}_\ell$ functions from the bi-orthogonal set of \mathcal{H} , i.e., $\langle \overline{h_k}; h_\ell \rangle_{\mathcal{S}} = \delta_{k,\ell}$ for any k, ℓ , with $\delta_{k,\ell}$ the Kronecker symbol. The mean $\mu_{\mathbf{I}}$ and the covariance $C_{\mathbf{I}}$ of $\mathbf{I}_\gamma \in \mathbb{C}^{3N_S}$ are defined then as

$$\mu_{\mathbf{I}}(\ell) = \mathbb{E}[\mathbf{I}_\gamma(\ell)] = \int_{\mathcal{G}} \mathbf{I}_\gamma(\ell) f_{\mathcal{G}}(\gamma) d\gamma, \quad (11)$$

$$C_{\mathbf{I}}(\ell, \ell') = \mathbb{E}[\mathbf{I}_\gamma(\ell) \mathbf{I}_\gamma^*(\ell')] - \mu_{\mathbf{I}}(\ell) \mu_{\mathbf{I}}^*(\ell'), \quad (12)$$

where $\mathbb{E}[\cdot]$ is the expectation operator with respect to γ , and $f_{\mathcal{G}}$ is the probability density function (PDF) of γ . In practice, the right-hand sides (rhs) of Eqs. (11)–(12) are computable by quadrature, as discussed in Section 5.1.

Then, using the eigenvalues $\lambda_1 \geq \dots \geq \lambda_{3N_S} \geq 0$ and the eigenvectors $\{\varphi_n\}_{n=1,\dots,3N_S}$ of $C_{\mathbf{I}}$, a Karhunen-Loève (KL) expansion is applied to \mathbf{I}_γ , which leads to [6, p. 17]

$$\mathbf{I}_\gamma(\ell) = \mu_{\mathbf{I}}(\ell) + \sum_{n=1}^{3N_S} \sqrt{\lambda_n} \rho_n(\gamma) \varphi_n(\ell), \quad \forall \gamma \in \mathcal{G}, \quad (13)$$

where, for any $n \geq 1$, the normalized KL variables

$$\rho_n(\gamma) = \frac{1}{\sqrt{\lambda_n}} \langle \mathbf{I}_\gamma - \mu_{\mathbf{I}}; \varphi_n \rangle_{\mathcal{S}} \quad (14)$$

are centered, with unit variances and mutually uncorrelated. Owing to the generally rapid decay of the eigenvalues λ_n , the sum in Eq. (13) can be truncated to a low order $N_{\text{KL}} \ll 3N_S$ and still yield a very accurate approximation of \mathbf{I}_γ in the \mathcal{L}^2 sense,

$$\mathbf{I}_\gamma(\ell) \approx \mu_{\mathbf{I}}(\ell) + \sum_{n=1}^{N_{\text{KL}}} \rho_n(\gamma) \sqrt{\lambda_n} \varphi_n(\ell). \quad (15)$$

By introducing $\rho_0 = 1$, $\lambda_0 = 1$, $\varphi_0 = \mu_{\mathbf{I}}$ and $\mathbf{J}_n(\mathbf{k}) = \sqrt{\lambda_n} \sum_{\ell=1}^{3N_S} \varphi_n(\ell) h_\ell(\mathbf{k})$, one obtains a representation of the form (7), i.e.,

$$\mathbf{J}_\gamma(\mathbf{k}) \approx \mathbf{J}_\gamma^{N_{\text{KL}}}(\mathbf{k}) = \sum_{n=0}^{N_{\text{KL}}} \rho_n(\gamma) \mathbf{J}_n(\mathbf{k}). \quad (16)$$

To completely characterize the randomness of $\mathbf{J}_\gamma^{N_{\text{KL}}}$, one needs to determine the *joint probability distribution* P_ρ of $\rho = (\rho_1, \dots, \rho_{N_{\text{KL}}})$, which are mutually uncorrelated but not necessarily statistically independent. Once P_ρ is known, the statistical post-processing of \mathbf{I}_γ becomes seamless. If \mathbf{I}_γ depends analytically on γ , P_ρ can be determined either analytically or by computing an empirical distribution at little numerical cost. In our case, where \mathbf{I}_γ depends numerically on γ , we apply a polynomial-chaos expansion to express ρ analytically in terms of γ and thereby ease the estimation of P_ρ .

3.2.1. Polynomial-chaos Expansion

Since all the components of ρ have finite variances, they can be expanded on a basis of orthogonal polynomials [6]. In addition to offering explicit analytical expressions of the random processes in terms of γ , polynomials have the advantage of an exponential convergence for functions that are infinitely differentiable. Hence,

$$\rho_\ell(\gamma) = \sum_{\mathbf{m} \in \mathbb{N}^d} c_\ell(\mathbf{m}) \psi_{\mathbf{m}}^d(\gamma), \quad \forall \ell = 1, \dots, N_{\text{KL}}, \quad (17)$$

$$\text{with } c_\ell(\mathbf{m}) = \mathbb{E} \left[\rho_\ell(\gamma) \psi_{\mathbf{m}}^d(\gamma) \right]. \quad (18)$$

The polynomials $\{\psi_{\mathbf{m}}^d(\gamma)\}_{\mathbf{m}}$ are d -variate, with d the dimension of \mathcal{G} , and mutually orthogonal with respect to the inner product defined by $f_{\mathcal{G}}$, i.e., $\mathbb{E} [\psi_{\mathbf{m}}^d(\gamma) \psi_{\mathbf{m}'}^d(\gamma)] = \delta_{\mathbf{m}\mathbf{m}'}$, for any $\mathbf{m}, \mathbf{m}' \in \mathbb{N}^d$ [23]. Eq. (18) shows that the computation of every $c_\ell(\mathbf{m})$ requires the availability of $\rho_\ell(\gamma)$ and a sampling strategy in \mathcal{G} . Trying to compute the PC coefficients $c_\ell(\mathbf{m})$ by quadrature breaks down rapidly as the order of the polynomials $\psi_{\mathbf{m}}^d(\gamma)$ or the dimension of \mathcal{G} increase. Higher PC orders are difficult to compute due to the finite degree of polynomial exactness of the integration rules, while increasing the dimension \mathcal{G} leads to a curse of dimensionality. Instead, since Eq. (17) is a linear equation in $c_\ell(\mathbf{m})$, it is solved for the PC coefficients using least-squares linear regression [24], as detailed in Section 4.1. Moreover, since the coefficients $\{c_\ell(\mathbf{m})\}_{\ell, \mathbf{m}}$ are deterministic, they can be pre-computed, stored and re-used for other incident fields.

For practical-implementation purposes, Eq. (17) is truncated to a finite order. We choose to apply an isotropic truncation by using the same order N_{PC} for all univariate polynomials and for all the KL variables, i.e.,

$$\rho_\ell(\gamma) \approx \sum_{\mathbf{m}=0}^{N_{\text{PC}}} \mathbf{c}(\mathbf{m}) \psi_{\mathbf{m}}^d(\gamma) = \sum_{j=1}^{N_{\text{coeff}}} \mathbf{c}[\mathbf{m}(j)] \psi_{\mathbf{m}(j)}^d(\gamma), \quad (19)$$

where $\mathbf{c}(\mathbf{m}) = [c_1(\mathbf{m}), \dots, c_{N_{\text{KL}}}(\mathbf{m})]$, $N_{\text{coeff}} = (N_{\text{PC}} + 1)^d$ is the number of PC coefficients, and the multi-indices are numbered through the bijection

$$\{1, \dots, N_{\text{coeff}}\} \ni j \mapsto \mathbf{m}(j) \in \{0, \dots, N_{\text{PC}}\}^d.$$

3.2.2. KLPC Expansion of the Current \mathbf{J}_γ

The KLPC approximation of \mathbf{J}_γ , derived from Eqs. (19) and (16), reads

$$\mathbf{J}_\gamma \approx \sum_{n=0}^{N_{\text{KL}}} \sum_{\mathbf{m}=0}^{N_{\text{PC}}} c_n(\mathbf{m}) \psi_{\mathbf{m}}^d(\gamma) \mathbf{J}_n. \quad (20)$$

This approximation captures the spatial dependency of \mathbf{J}_γ *deterministically* via the eigenfunctions of the covariance, and the randomness of \mathbf{J}_γ *analytically* through the PC approximation of ρ . Since the KLPC model is analytical, P_ρ can be estimated by generating a large ensemble of samples of ρ at a negligible numerical cost.

4. ADAPTIVE IMPLEMENTATION OF THE KLPC MODEL

With the stochastic model now established, two major aspects need to be considered, viz. 1) the method for computing the PC expansion, and 2) the method for determining the orders of the KL and PC expansions to ensure the accuracy of the resulting KLPC probability distribution.

4.1. Estimated Accuracy of the PC Expansion for a Fixed KL Order

Since Eq. (19) is linear in $\mathbf{c}(\mathbf{m})$, the PC coefficients are computed by least-squares (LS) linear regression. For a given KL expansion of order N_{KL} , the LS problem is formulated as

$$\Psi_{\text{PC}}(\mathcal{G}_{\text{Reg}}) C_{\text{KP}} = \mathbf{P}(\mathcal{G}_{\text{Reg}}), \quad (21)$$

with $\mathcal{G}_{\text{Reg}} = \{\gamma_k\}_{k=1, \dots, N_{\text{Reg}}} \subset \mathcal{G}$ the regression set, $\Psi_{\text{PC}}(\mathcal{G}_{\text{Reg}}) = \left[\psi_{\mathbf{m}(j)}^d(\gamma_i) \right]_{1 \leq i \leq N_{\text{Reg}}, 1 \leq j \leq N_{\text{coeff}}}$ and $C_{\text{KP}} = (c_\ell[\mathbf{m}(j)])_{1 \leq \ell \leq N_{\text{KL}}; 1 \leq j \leq N_{\text{coeff}}}$ the KL coefficients to be determined. The rhs $\mathbf{P}(\mathcal{G}_{\text{Reg}}) = [\rho_j(\gamma_i)]_{1 \leq i \leq N_{\text{Reg}}, 1 \leq j \leq N_{\text{KL}}}$ is evaluated using Eq. (14). Solving Eq. (21) for C_{KP} yields the estimate

$$C_{\text{KP}} \approx (\Psi_{\text{PC}}^t \Psi_{\text{PC}})^\dagger \Psi_{\text{PC}}^t \mathbf{P}, \quad (22)$$

with (\dagger) the pseudo-inverse operator. Only one inversion of Ψ_{PC} is required for every set \mathcal{G}_{Reg} . Increasing N_{KL} only increases the dimension of $\mathbf{P}(\mathcal{G}_{\text{Reg}})$ while leaving $\Psi_{\text{PC}}(\mathcal{G}_{\text{Reg}})$ (to be inverted) unchanged. Thus, our algorithm is rather insensitive to the number of KL variables, which is advantageous for the parallelized computation of multiple PC spectra. To ensure the accuracy of the estimate, and given our limit to the number of function evaluations (N_{MAX}), we conservatively use $3N_{\text{coeff}}$ samples in the LS algorithm as long as $3N_{\text{coeff}} \leq N_{\text{MAX}}$, otherwise we use $2N_{\text{coeff}}$ samples as long as $2N_{\text{coeff}} \leq N_{\text{MAX}}$. Hence, the highest PC order that can be considered is

$$N_{\text{PC}, \text{max}} = \left\lfloor \left(\frac{N_{\text{MAX}}}{2} \right)^{1/\dim(\mathcal{G})} - 1 \right\rfloor. \quad (23)$$

The power of a PC approximation of order N_{PC} , viz.

$$\mathcal{N}_3(\mathbf{c}_\ell) = \sqrt{\sum_{j=1}^{N_{\text{coeff}}} |c_\ell[\mathbf{m}(j)]|^2} \quad (24)$$

is compared to 1, i.e., the theoretical variance of ρ_ℓ . Thus, given a tolerance $\varepsilon_{\text{PC}, \text{max}}$, the KL coefficients that verify $|\mathcal{N}_3(\mathbf{c}_\ell) - 1| \leq \varepsilon_{\text{PC}, \text{max}}$ are assumed to be sufficiently accurately approximated by the PC expansion.

4.2. Adaptive KLPC Decomposition

It is common practice to truncate the KL approximation based on the decay of the eigenvalues of $\mathbf{C}_\mathbf{I}$. For instance, given a threshold $\tau_{\text{KL}} > 0$, one finds the order N_{L2} as the smallest integer such that

$\sum_{k > N_{\text{L2}}} \lambda_k / \sum_{k \geq 1} \lambda_k < \tau_{\text{KL}}$. While such an approach ensures the accurate restitution of the variance of the observable to within τ_{KL} , it does not guarantee the accuracy of higher-order moments. To tackle this issue, we propose an adaptive scheme that uses higher-order statistics of a canonical observable, as illustrated by Fig. 3.

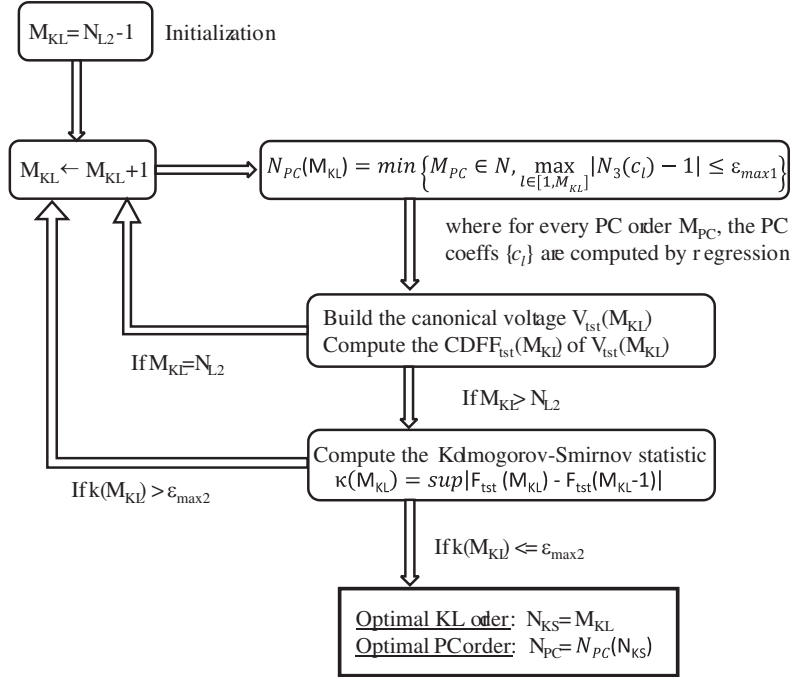


Figure 3. Flow-chart showing the adaptive determination of the orders of the KL and PC expansions.

First, the PC expansion is computed for $M_{\text{KL}} = N_{\text{L2}}$ KL variables. The accuracy of the PC approximation of the coefficients c_ℓ is assessed by verifying that $|\mathcal{N}_3(\mathbf{c}_\ell) - 1| \leq \varepsilon_{\text{PC,max}}$ (see Eq. (24)), for a given tolerance $\varepsilon_{\text{PC,max}}$. Next, the canonical variable

$$V_{\text{tst}}(M_{\text{KL}}) = \sum_{n=1}^{M_{\text{KL}}} \sqrt{\lambda_n} |\rho_n(\alpha)|^2 \geq 0 \quad (25)$$

is considered. This variable can be regarded as the voltage induced on a wire on which flows the current $\mathbf{J}_\alpha - \mu_{\mathbf{J}}$ by an incident field $\mathbf{E}_{\text{tst}} = \sum_{n=1}^{M_{\text{KL}}} \rho_n^*(\alpha) \varphi_n^*$. The CDF of $V_{\text{tst}}(M_{\text{KL}})$, denoted $F_{M_{\text{KL}}}$, is readily available via sampling the PC expansion. This procedure is then repeated for $M_{\text{KL}} \leftarrow M_{\text{KL}} + 1$ and the CDFs $F_{M_{\text{KL}}}$ and $F_{M_{\text{KL}}-1}$ are compared using the Kolmogorov-Smirnov (KS) statistic [25, p. 316]

$$\kappa(M_{\text{KL}}) = \sup_{v \geq 0} |F_{M_{\text{KL}}}(v) - F_{M_{\text{KL}}-1}(v)|. \quad (26)$$

This quantifies the difference in higher-order statistics due to the increasing order of the KL expansion. The value of M_{KL} is incremented until $\kappa(M_{\text{KL}})$ drops below a threshold ε_{KS} chosen by the modeler. The resulting optimal KL order is denoted N_{KS} . It is worth noting that, whenever M_{KL} is increased, the order of the PC expansion is increased until all M_{KL} KL variables are accurately expanded following the rationale of Section 4.1.

The numerical efficiency of this approach hinges on two choices that we make. First, since our implementation of the PC-projection algorithm is insensitive to the number of KL variables being computed (see Section 4.1), we simultaneously compute the PC projections of multiple KL variables with the same regression set \mathcal{G}_{Reg} . Our second choice is motivated by the fact that solving Eq. (21) every time the KL or PC orders are increased can become numerically cumbersome. Instead, we compute the PC spectra of a super-set of $M_{\text{KL,max}}$ KL variables simultaneously and verify the accuracy of the subset of M_{KL} variables of interest. Only when the M_{KL} variables are not accurate in RMS sense (i.e., there is at least one $\ell \in \{1, \dots, M_{\text{KL}}\}$ such that $|\mathcal{N}_3(\mathbf{c}_\ell) - 1| > \varepsilon_{\text{PC,max}}$) is the order N_{PC} increased and the PC projection recomputed, by LS regression, for the super-set of $M_{\text{KL,max}}$ KL variables. Both choices strongly help the computational efficiency of this approach as will be shown in Section 5.2. To

the best of the authors’ knowledge, this is a novel approach to perform KL and PC expansions jointly and adaptively.

5. KLPC EXPANSION OF THE CURRENT DISTRIBUTION

We now apply our KLPC method to the stochastic thin-wire setup described in Section 2.1. We recall that this problem involves three random parameters, viz. $\gamma = (\alpha_1^x, \alpha_1^z, \xi)$, which are assumed mutually statistically independent with uniform distributions in their ranges. To apply the spectral reformulation at the core of our stochastic method, the domain \mathcal{S} is sampled into the wave-vectors $\mathbf{k}_{i,\ell} = (2\pi/\lambda)\mathbf{u}_r(\theta_i, \phi_\ell)$ (see Eq. (3)), with

$$\theta_i = \arccos\left(\frac{i}{N_1}\right), \quad \phi_\ell = \frac{\pi}{2}\left(\frac{\ell-1}{N_1} - 1\right), \quad (27)$$

where $i = 1, \dots, N_1 - 1$ and $\ell = 1, \dots, 2N_1 + 1$ with $N_1 = 10$. This results in a discrete sampling of \mathcal{S} into $N_{\text{dir}} = (N_1 - 1)(2N_1 + 1) = 189$ directions of incidence. The expansion and testing functions ($\{h_\ell\}_\ell$ and $\{\overline{h}_\ell\}_\ell$) over \mathcal{S} are chosen as delta functions and the functions defined on \mathcal{S} are approximated by point-matching, i.e., $\mathbf{E}_\beta(\mathbf{k}_{i,\ell})$ and $\mathbf{J}_\gamma(\mathbf{k}_{i,\ell})$ are represented by $(3N_{\text{dir}})$ -dimensional vectors. As an indication, using the deterministic model with the axis of W_α subdivided into $N_{\text{seg}} = 224$ segments, the computation of the voltage induced by a single plane wave (the superposition of all N_{dir} plane waves) requires ~ 218 ms (~ 340 ms) on a 2.7 GHz computer with an Intel Core i7 processor. Thus, most of the computational effort is devoted to the build-up of the impedance matrix in the MoM and its LU factorization.

5.1. Second-Order Statistical Moments

The mean $\mu_{\mathbf{I}}$ and covariance $C_{\mathbf{I}}$ in Eqs. (11) and (12) are computed using a sparse-grid (SG) quadrature rule, which is well suited to handle integrals over multi-dimensional domains and takes advantage of the smoothness of the integrands [26]. As a reference, a Monte-Carlo (MC) algorithm is also used. Both of these quadrature rules are known to mitigate the effects of the ‘‘curse of dimensionality’’, i.e., the exponentially-growing complexity as a function of the dimension of the sampling space. More advanced sampling schemes, e.g., with adaptive dimensionality reduction, could also be considered [8, 9].

Since $C_{\mathbf{I}}$ is a higher-order moment than $\mu_{\mathbf{I}}$, its computation is more demanding. Hence, the convergence of the quadrature estimates is monitored through the relative variations of $C_{\mathbf{I}}$ in terms of its Fr obenius norm [27, p. 55], as the complexity of the quadrature increases. Table 1 shows the relative error of $C_{\mathbf{I}}$ versus the complexity N_{quad} of the quadrature rule. For both algorithms, $C_{\mathbf{I}}$ can be obtained with a relative accuracy better than 0.1% (even $\sim 0.01\%$ for the SG rule) with $\sim 10^3$ samples.

Table 1. Convergence of the Monte-Carlo and sparse-grid estimates of the covariance matrices $C_{\mathbf{I}}$ (random geometry) and $C_{\mathbf{E}}$ (random incident field studied in Section 6.2). Number N_{-k} of function evaluations required to reach target accuracy $\varepsilon_{\text{rel}} \leq \varepsilon_{\text{max}} = 10^{-k}$, and relative error $\varepsilon_{\text{rel}}(N_{-k})$.

	Computation of $C_{\mathbf{I}}$		Computation of $C_{\mathbf{E}}$	
	Sparse grids	Monte-Carlo	Sparse grids	Monte-Carlo
$N_{-2} = N_{\text{quad}}(\varepsilon_{\text{rel}} \leq 10^{-2})$	441	129	137	513
$\varepsilon_{\text{rel}}(N_{-2})$	$3.2 \cdot 10^{-3}$	$4.4 \cdot 10^{-3}$	$2.8 \cdot 10^{-3}$	$1.8 \cdot 10^{-3}$
$N_{-3} = N_{\text{quad}}(\varepsilon_{\text{rel}} \leq 10^{-3})$	1073	1025	401	1025
$\varepsilon_{\text{rel}}(N_{-3})$	$1.2 \cdot 10^{-4}$	$8.2 \cdot 10^{-4}$	$1.7 \cdot 10^{-5}$	$7.5 \cdot 10^{-4}$

Next, $C_{\mathbf{I}}$ is spectrally decomposed using an eigenvalue solver (e.g., F02GCF of the LAPACK library) [27, p. 393]. The numerical cost of this decomposition scales as $\sim (3N_{\text{dir}})^3$ and requires ~ 12 s. The largest eigenvalues, normalized by the trace of $C_{\mathbf{I}}$, are listed in Table 2. The decay of the eigenvalues is rapid since the first four eigenvalues capture more than $\tau_{\text{KL}} = 99.9\%$ of the trace of $C_{\mathbf{I}}$, i.e., $N_{L2} = 4$.

5.2. KLPC Decomposition of \mathbf{J}_γ

Since all the random input parameters in this article follow a uniform probability distribution, it is natural to consider a Legendre-uniform polynomial chaos [28]. The Legendre polynomials are obtained recursively [23, p.333]. The orders of the KL and PC expansions are determined adaptively according

Table 2. Main eigenvalues of the covariance $C_{\mathbf{I}}$ normalized by $\text{Tr}(C_{\mathbf{I}})$ (left two columns), and similarly for $C_{\mathbf{E}}$ (right two columns)

k	Eigenvalues of $C_{\mathbf{I}}$ with $\text{Tr}(C_{\mathbf{I}}) = 1.652 (\text{A} \cdot \text{m}^{-1})^2$		Eigenvalues of $C_{\mathbf{E}}$ with $\text{Tr}(C_{\mathbf{E}}) = 5.827 \cdot 10^{-3} (\text{V} \cdot \text{m}^{-1})^2$	
	$\lambda_k^2/\text{Tr}(C_{\mathbf{I}})$	$1 - \sum_{\ell=1}^k \lambda_\ell^2/\text{Tr}(C_{\mathbf{I}})$	$\lambda_k^2/\text{Tr}(C_{\mathbf{E}})$	$1 - \sum_{\ell=1}^k \lambda_\ell^2/\text{Tr}(C_{\mathbf{E}})$
1	$9.810 \cdot 10^{-1}$	$1.903 \cdot 10^{-2}$	$5.912 \cdot 10^{-1}$	$4.088 \cdot 10^{-1}$
2	$1.571 \cdot 10^{-2}$	$3.324 \cdot 10^{-3}$	$4.085 \cdot 10^{-1}$	$2.776 \cdot 10^{-4}$
3	$2.069 \cdot 10^{-3}$	$1.255 \cdot 10^{-3}$	$2.142 \cdot 10^{-4}$	$6.338 \cdot 10^{-5}$
4	$1.236 \cdot 10^{-3}$	$1.860 \cdot 10^{-5}$	$4.754 \cdot 10^{-5}$	$1.585 \cdot 10^{-5}$
5	$1.207 \cdot 10^{-5}$	$6.523 \cdot 10^{-6}$	$1.288 \cdot 10^{-5}$	$2.965 \cdot 10^{-6}$
6	$4.951 \cdot 10^{-6}$	$1.572 \cdot 10^{-6}$	$2.863 \cdot 10^{-6}$	$1.020 \cdot 10^{-7}$
7	$8.582 \cdot 10^{-7}$	$7.138 \cdot 10^{-7}$	$4.170 \cdot 10^{-8}$	$6.031 \cdot 10^{-8}$

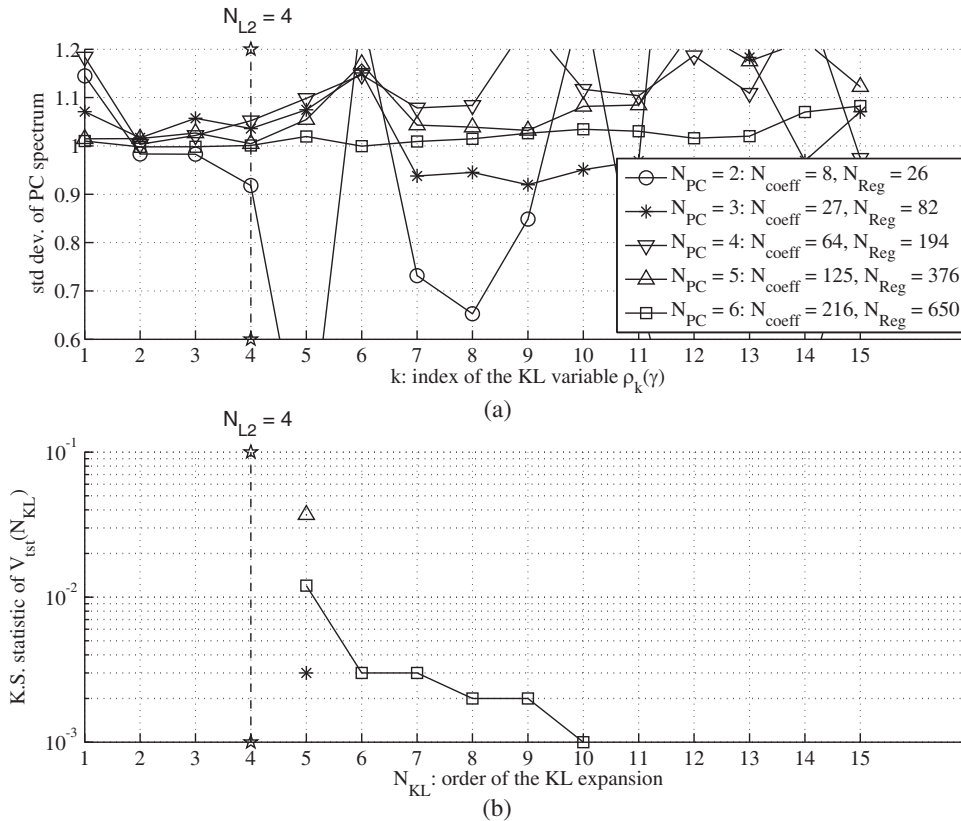


Figure 4. Variance- and KS-based adaptive determination of the KL and PC orders for \mathbf{J}_γ : (a) variances of the first 15 KL variables as a function of the order N_{PC} of the PC expansion. (b) Value of the K.S. statistic of V_{tst} for PC expansions that are accurate in terms of the variance.

to the scheme described in Section 4.2. Thus, we simultaneously compute the PC spectra of a superset consisting of the first $M_{\text{KL,max}} = 15$ KL variables, i.e., more than the $N_{\text{L2}} = 4$ variables prescribed by the decay of the eigenvalues. Since $\dim(\mathcal{G}) = 3$ (i.e., $\gamma = (\alpha_1^x, \alpha_1^z, \xi)$) and given our limit to the number of function evaluations of $N_{\text{MAX}} = 2000$, Eq. (23) indicates that the highest order of PC expansion we can consider is $N_{\text{PC,max}} = 9$.

The top part of Fig. 4 displays the variances of the KL variables after applying PC expansions of increasing orders. The number N_{coeff} of PC coefficients per KL variable is indicated in the legend, as well as the number N_{Reg} of samples used to estimate the PC coefficients by LS regression. After every PC expansion, the variance of each KL variable is compared to its theoretical value of 1, with a maximum tolerance of $\varepsilon_{\text{PC,max}} = 0.1$. One could consider a tighter threshold at the expense of a larger computational burden. With these criteria, according to Fig. 4(a), to estimate the first $N_{\text{L2}} = 4$ KL variables accurately, one needs to use $N_{\text{PC}} = 3$, since for $N_{\text{PC}} = 2$ the variance of ρ_1 is 1.145 and the deviation from 1 is larger than $\varepsilon_{\text{PC,max}}$. Once the N_{L2} variables are accurately determined, they are used to build the CDF of the canonical voltage $V_{\text{tst}}(N_{\text{L2}})$, which is stored.

Next, the number of KL variables is increased to $M_{\text{KL}} = N_{\text{L2}} + 1 = 5$. As the variances of $\{\rho_1, \dots, \rho_5\}$ are already accurate with $N_{\text{PC}} = 3$, a new PC projection is not required and these PC coefficients can be used to obtain the CDF of $V_{\text{tst}}(M_{\text{KL}})$ and compute the corresponding KS statistic $\kappa(M_{\text{KL}})$, which is shown in Fig. 4(b) and equal to $3 \cdot 10^{-3}$. Since this value is larger than the threshold $\varepsilon_{\text{KS}} = 10^{-3}$, more KL variables must be included in the analysis, and therefore M_{KL} is increased to $N_{\text{L2}} + 2 = 6$.

The process described in the previous paragraph is iterated and, as shown in Fig. 4, it converges when $N_{\text{KS}} = 10$ KL variables are included in the KL expansion, for which one needs a PC expansion of order $N_{\text{PC}} = 6$ (mainly due to the slow convergence of the PC expansion of ρ_6). This amounts to $N_{\text{coeff}} = 216$ PC coefficients per KL variable, for which we use $N_{\text{Reg}} = 650$ random samples in the least-squares estimation process.

With the KLPC expansion at hand, the probability distribution P_ρ of the vector of dominant KL variables $\rho = (\rho_1, \dots, \rho_{N_{\text{KS}}})$ is approximated via Eq. (19) by generating a large set of samples of ρ at minimal cost: for instance, computing 10^4 samples for ρ requires merely ~ 2 s.

6. VOLTAGE INDUCED BY ARBITRARY INCIDENT FIELDS

The KLPC model is now used to estimate the PDF of the voltage induced at the port of the wire by arbitrary combinations of plane waves with their supports in \mathcal{S} . Using Eq. (2), the polarizations of the incident fields are defined as the following Gaussian beams [29]

$$\mathbf{E}_\beta(\mathbf{k}_i, \eta) = \omega_\beta(\mathbf{k}_i) E_0 [\mathbf{e}_d(\mathbf{k}_i, \eta) + \mathbf{e}_m(\mathbf{k}_i, \eta)], \quad \forall \mathbf{k}_i \in \mathcal{S}, \quad (28)$$

with $E_0 = 1 \text{ V} \cdot \text{m}^{-1}$, and η the polarization angle of the incident field. The unit vector $\mathbf{e}_d(\mathbf{k}_i, \eta)$ indicates the polarization of the “direct” plane wave, i.e., propagating along the direction \mathbf{k}_i , with a polarization angle η . Similarly, $\mathbf{e}_m(\mathbf{k}_i, \eta)$ is a unit vector directed along the polarization of the mirror-imaged plane wave induced by the presence of the PEC ground plane. The Gaussian weighting function ω_β is given by

$$\omega_\beta(\mathbf{k}_i) = \omega_0 \exp\left(-\frac{1}{2\sigma_0} \frac{|\mathbf{k}_i \times \mathbf{k}_0|^2}{|\mathbf{k}_i \cdot \mathbf{k}_0|^2}\right), \quad (29)$$

with $\mathbf{k}_0 = (2\pi/\lambda)\mathbf{u}_r(\theta_0, \phi_0)$ the mean wave-vector, σ_0 the width, and ω_0 a normalizing factor such that the integral of ω_β over \mathcal{S} equals 1.

6.1. Deterministic Incident Fields

We first consider deterministic incident fields. This situation arises when assessing the effects of production drifts on the performance of a device placed in various prescribed electromagnetic environments. This is also relevant for remote sensing where, often, the characteristics of the source of the incident field, e.g., a radar, are known, whereas geometrical or physical properties of the target are unknown. The testing fields considered are

- *Field \mathbf{E}_1* : a combination of parallel-polarized ($\eta = 90^\circ$) waves, centered around $(\theta_0 = 60^\circ, \phi_0 = -45^\circ)$, with a width $\sigma_0 = 0.2$;
- *Field \mathbf{E}_2* : a combination of parallel-polarized ($\eta = 90^\circ$) waves, centered around $(\theta_0 = 45^\circ, \phi_0 = 45^\circ)$, with a width $\sigma_0 = 0.1$;
- *Field \mathbf{E}_3* : a combination of perpendicular-polarized ($\eta = 0^\circ$) waves, centered around $(\theta_0 = 45^\circ, \phi_0 = 0^\circ)$, with a width $\sigma_0 = 0.1$.

The amplitudes of these fields are plotted in Fig. 5 (left column). For each of these incident fields, the PDFs of the real and imaginary parts of the induced voltage V are determined using 1) a set of $N_{\text{emp}} = 10^4$ random realizations of the deterministic model (i.e., by evaluating Eq. (4)) and taking this set as a reference, 2) the \mathcal{L}^2 -based KLPC expansion that uses $N_{L2} = 4$ KL variables, and 3) the higher-order KL expansion that uses $N_{KS} = 10$ KL variables. The results, plotted in Fig. 5 (middle and right columns), show the varying levels of accuracy of the \mathcal{L}^2 -KLPC model depending on the incident field. For instance, with \mathbf{E}_1 or \mathbf{E}_3 , the \mathcal{L}^2 -KLPC expansion yields an accurate approximation of the distribution of $\text{Re}(V)$. However, differences can be noted in the shapes of the PDF of $\text{Re}(V)$ induced by \mathbf{E}_2 , and the PDFs of $\text{Im}(V)$. In contrast, the higher-order KLPC approximation is accurate in terms of the shape and the support of the PDFs of $\text{Re}(V)$ and $\text{Im}(V)$.

The KLPC approach is also advantageous for its computation time as shown in Table 3: once the initial effort has been devoted to building the KLPC model (in ~ 13 mins), subsequent uses of this

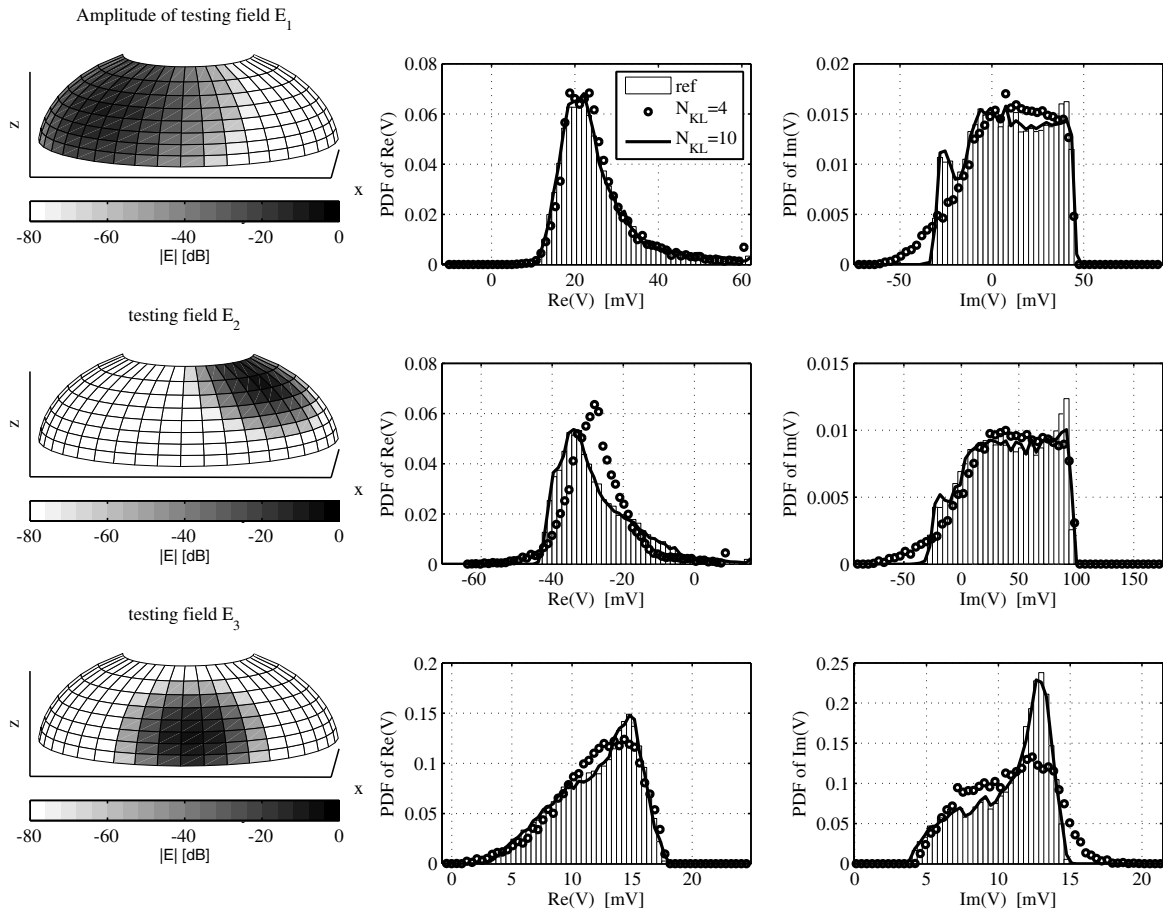


Figure 5. PDFs of the real (middle column) and imaginary (right column) parts of V induced by three combinations of plane waves (the amplitudes of the incident fields are shown in the left column). The PDFs are obtained from 10^4 samples of the initial model (empirical PDF as histogram), and from KLPC expansions using N_{L2} (circles) and N_{KS} (solid line) KL variables.

Table 3. Detail of the computation time for the KLPC approach and the systematic use of the initial model (i.e., without the KLPC expansion).

	Computation time [s]	
	random \mathbf{J}_γ	random \mathbf{E}_β
$T_{\text{pre},1}$: Computation of mean & covariance	324	258
$T_{\text{pre},2}$: Eigen-decomposition of covariance	13	15
$T_{\text{pre},3}$: PC projection of KL variables	249	66
$T_{\text{pre,KLPC}} = T_{\text{pre},1} + T_{\text{pre},2} + T_{\text{pre},3}$	586	339
$T_{1,\text{KLPC}}$: single KLPC evaluation	2.0×10^{-4}	
KLPC evaluations N_{samp} samples	$\sim T_{\text{pre,KLPC}} + N_{\text{samp}} T_{1,\text{KLPC}}$	
$N_{\text{samp}} = 10^5$	610	362
Initial model without any expansion (1 sample)	$T_{1,\text{NI}} \sim 0.340$	
N_{samp} samples	$\sim N_{\text{samp}} \times T_{1,\text{NI}}$	
$N_{\text{samp}} = 10^5$	~ 9.4 hours	

model come at very little numerical cost (~ 2 s to compute the 10^4 voltage samples per incident field). This is significantly less than the ~ 30 min required to compute the reference PDF for each incident field via the deterministic model.

6.2. Stochastic Incident Field

The KLPC approach can also be used to characterize a random incident field and determine its interaction with arbitrary receivers. This application is relevant, e.g., for mode-stirred-chamber problems where the field in the test volume is best described as stochastic. Using Eqs. (28) and (29), the stochastic incident field \mathbf{E}_β considered here has a random amplitude $E_0 \in [0.5, 3] \text{ V} \cdot \text{m}^{-1}$, a random polarization defined by the angle $\eta_0 \in [0^\circ, 90^\circ]$ and a Gaussian weighting of deterministic width $\sigma_0 = 3$ but random mean direction of incidence given by $\theta_0 \in [30^\circ, 60^\circ]$ and $\phi_0 \in [-45^\circ, 45^\circ]$.

The vector $\beta = (E_0, \theta_0, \phi_0, \eta_0)$ of uncertain parameters is assumed random with mutually independent uniformly distributed components. Although the dimension of β is higher than the dimension of $\gamma = (\alpha, \xi)$, the dependence of \mathbf{E}_β on β is significantly smoother than the dependence of \mathbf{J}_γ on γ at the resonance frequency $f_1 = 1997$ GHz. When computing the mean $\mu_{\mathbf{E}}$ and covariance $C_{\mathbf{E}}$ by quadrature, the sparse-grid rule takes advantage of this smoothness, unlike the Monte-Carlo rule, as shown in Table 1 (right two columns containing the results for $C_{\mathbf{E}}$). The smoothness of \mathbf{E}_β in terms of β translates also in a rapid decay of the eigenvalues of $C_{\mathbf{E}}$ (see Table 2, right two columns): $N_{\text{L2}} = 2$ eigenvalues account for more than 99.9 % of the trace of $C_{\mathbf{E}}$. The KLPC expansion of \mathbf{E}_β is done adaptively, with a canonical voltage V_{tst} defined using the eigenvectors and eigenvalues of $C_{\mathbf{E}}$ in Eq. (25). The resulting model comprises $N_{\text{KS}} = 7$ KL variables expressed via a PC expansion of order $N_{\text{PC}} = 3$, i.e., $N_{\text{coeff}} = 81$ PC coefficients per KL variable, computed using $N_{\text{LS}} = 244$ samples in the LS regression.

This KLPC model of the random \mathbf{E}_β is combined with the KLPC model of the random wire of Section 5 to characterize the voltage induced by their mutual interaction. This problem involves seven random parameters, viz. $(\alpha^x, \alpha^z, \xi, E_0, \theta_0, \phi_0, \eta_0)$. The KLPC approximations of \mathbf{J}_γ and \mathbf{E}_β are

$$\mathbf{J}_\gamma \approx \sum_{n=0}^{N_{\text{KS},J}} \rho_{J,n}(\gamma) \sqrt{\lambda_{J,n}} \varphi_{J,n}, \quad \mathbf{E}_\beta \approx \sum_{m=0}^{N_{\text{KS},E}} \rho_{E,m}(\beta) \sqrt{\lambda_{E,m}} \varphi_{E,m}, \quad (30)$$

with $\rho_{J,0} = \rho_{E,0} = \lambda_{J,0} = \lambda_{E,0} = 1$, $\varphi_{J,0} = \mu_{\mathbf{I}}$, $\varphi_{E,0} = \mu_{\mathbf{E}}$, and $\{\lambda_{J,n}, \varphi_{J,n}\}_{n \geq 1}$ and $\{\lambda_{E,m}, \varphi_{E,m}\}_{m \geq 1}$ the eigen-systems of $C_{\mathbf{I}}$ and $C_{\mathbf{E}}$, respectively. The orders of the KL expansions of \mathbf{J}_α and \mathbf{E}_β are $N_{\text{KS},J} = 9$ and $N_{\text{KS},E} = 7$, respectively. The KLPC model of the induced voltage is obtained by

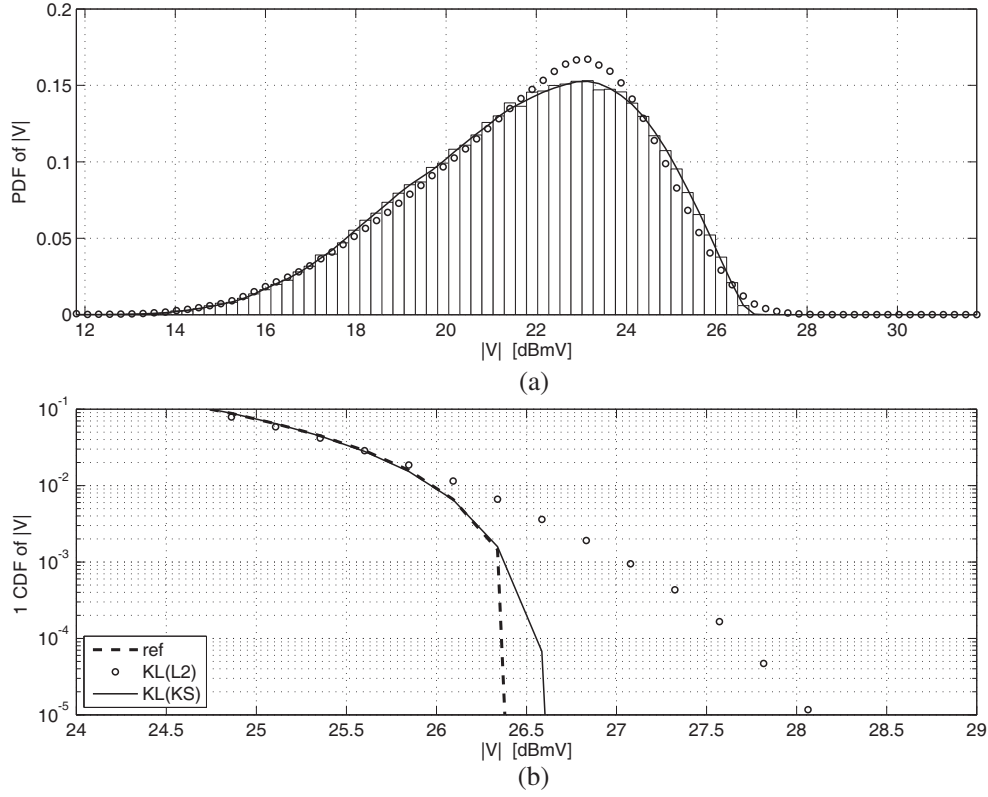


Figure 6. (a) PDF and (b) complementary CDF of the amplitude of the voltage induced by the random incident field at the port of the random wire, as obtained from 10^5 samples (ref), the variance based KLPC expansion [KL(L2)] and the adaptive higher-order KLPC expansion [KL(KS)].

inserting Eq. (30) in Eq. (4), i.e.,

$$V(\gamma, \beta) \approx - \sum_{n=0}^{N_{KS,J}} \sum_{m=0}^{N_{KS,E}} \sqrt{\lambda_{J,n} \lambda_{E,m}} G_{J,E}(m, n) \rho_{J,n}(\gamma) \rho_{E,m}(\beta). \quad (31)$$

The matrix $G_{J,E} = (\langle \varphi_{J,n}; \varphi_{E,m} \rangle_{\mathcal{S}})_{n,m}$ captures the spatial correlation between the two sets of eigenfunctions, while the product $\sqrt{\lambda_{J,n} \lambda_{E,m}}$ acts as a physical weight and the KL variables carry the randomness.

Another advantage of the Eq. (31) is that with merely N_{MC} random realizations of γ and N_{MC} random realizations of β , one gets N_{MC}^2 random realizations of V , for the computation time required to run the KLPC models $2N_{MC}$ times. To keep the problem manageable, we only use 10^5 samples of the deterministic model (computed in ~ 8.5 hours) as a reference for comparisons against the distributions of $V_{L2} = V_{N_{L2,J}, N_{L2,E}}$ and $V_{KS} = V_{N_{KS,J}, N_{KS,E}}$. Fig. 6(a) shows that V_{L2} already produces an accurate approximation of the PDF of $|V|$ despite an overshoot at the mode of the distribution, around 23 dBmV. Since the distribution is plotted for $|V|$ on a logarithmic scale, the shape of the distribution is the same for the received power $P = |V|^2/2$ induced at the port of the wire, albeit with a shifted support. As a practical application of the statistics at hand, we determined the probability of exceedance of $|V|$ by analyzing the complementary CDF, i.e., $1 - F_{|V|}$. Fig. 6(b) illustrates the limited error that is made to estimate these probabilities of exceedance when using V_{KS} rather than V_{L2} .

7. COMPUTATION TIME

Besides its accuracy, the main advantage of the KLPC method is its computational efficiency for multiple evaluations of the observable. Indeed, the KLPC computation time consists of a pre-computation stage

that needs to be invested in only once, followed by evaluations of the thus obtained KLPC model. The pre-computations start with the determination of the mean and covariance operators by quadrature, the efficiency of which depends on the smoothness of the dependence of the integrand with respect to the stochastic parameters. This is well illustrated in Tables 1 and 3, where the slower convergence of the computation of $C_{\mathbf{I}}$ compared to $C_{\mathbf{E}}$ is due to the rougher behavior of \mathbf{L}_γ versus γ caused by the resonances.

The spectral decomposition of the covariance matrix requires ~ 14 s for this problem and this cost evolves with the cube of the dimension of the stochastic tensor, i.e., $(3N_{\text{dir}})^3$. Since the PC decomposition of the dominant KL variables by linear regression involves a singular-value decomposition, the complexity of this task evolves as $\sim N_{\text{coeff}}^3 = (N_{\text{PC},1})^{3\dim(\mathcal{G})}$, where $N_{\text{PC},1}$ is the order of the univariate PC expansions. All these factors contribute to a total pre-computation time $T_{\text{pre,KLPC}}$ that ranges from 339 s (~ 5.6 min) to 586 s (~ 10 min), as reported in Table 3.

After this numerical investment, the evaluations of the KLPC model of the observable merely require $T_{1,\text{KLPC}} \sim 0.2$ ms, which is three orders of magnitude smaller than the $T_{1,\text{NI}} \sim 345$ ms required to evaluate the observable via the initial model. For instance, generating an ensemble of N_{samp} realizations of the observable will require $N_{\text{samp}}T_{1,\text{NI}}$ seconds with the initial model, versus $T_{\text{pre,KLPC}} + N_{\text{samp}}T_{1,\text{KLPC}}$ seconds in the KLPC approach. Table 3 shows that, already with a single incident field, the KLPC approach outperforms the brute-force approach when it comes to computing the distribution of the induced voltage using $N_{\text{samp}} = 10^5$ samples.

8. CONCLUSION

We have presented a method for characterizing stochastic linear observables that describe electromagnetic interactions between a randomly shaped material object and arbitrary incident fields. The stochastic approach hinges on the accurate computation of the mean and covariance of the stochastic tensors by quadrature, the spectral decomposition of the covariance and the projection on a set of orthogonal polynomials by linear regression. Even though the covariance operators of the electromagnetic fields and current distributions are not compact in general, which is a prerequisite for the spectral decomposition, our method uses a point-spectrum regularization to cast the problem in terms of compact operators. A spectral reformulation of the observable allowed us to separate the effects of the randomness of the scatterer from the randomness of the incident field.

Our implementation of the polynomial-chaos projection is optimized to compute multiple PC projections simultaneously, which makes it a good candidate for parallelization. We have presented an adaptive algorithm to determine the orders of the KL and PC expansions jointly and adaptively using higher-order statistics. Such a rationale refines the common approach that truncates the KL expansion using only the decay of the eigenvalues of the covariance. Our KLPC model provides a complete statistical toolbox to approximate the probability distribution of the observable accurately.

The results obtained for the example of the voltage induced at the port of a stochastic thin-wire frame by arbitrary combinations of plane waves show the high accuracy and numerical efficiency of the proposed method, thereby justifying the numerical investment in the construction of the KLPC model. While this article was illustrated by examples inspired from EMC, the stochastic rationale can be applied straightforwardly to antenna-design and scattering problems, where linear observables are also used. This semi-intrusive method is well suited for mode-stirred-chamber problems as it allows to characterize the randomness of the chamber once and then use the KLPC model to obtain the distribution of voltages induced at the ports of equipments under test.

ACKNOWLEDGMENT

This work was funded by the Dutch Ministry of Economic Affairs, in the Innovation Research Program (IOP) number EMVT 04302.

REFERENCES

1. Holland, R. and R. St. John, *Statistical Electromagnetics*, CRC Press, 1999.

2. Meng, Y. and Y. Shan, "Measurement uncertainty of complex-valued microwave quantities," *Progress In Electromagnetics Research*, Vol. 136, 421–433, 2013.
3. Michielsen, B. and C. Fiachetti, "Covariance operators, Green functions, and canonical stochastic electromagnetic fields," *Radio Science*, Vol. 40, No. 5, RS5001.1–RS5001.12, 2005.
4. Lemoine, C., E. Amador, and P. Besnier, "On the K-factor estimation for Rician channel simulated in reverberation chamber," *IEEE Trans. on Antennas and Propagation*, Vol. 59, No. 3, 1003–1012, 2011.
5. Phelps, R., M. Krasnicki, R. Rutenbar, L. Carley, and J. Hellums, "Anaconda: Simulation-based synthesis of analog circuits via stochastic pattern search," *IEEE Transactions on Computer-Aided Design of Integrated Circuits and Systems*, Vol. 19, No. 6, 703–717, Jun. 2000.
6. Ghanem, R. and P. Spanos, *Stochastic Finite Elements: A Spectral Approach*, Dover Publications, 1991.
7. Vaessen, J., O. Sy, M. van Beurden, and A. Tijhuis, "Monte-Carlo method applied to a stochastically varying wire above a PEC ground plane," *Proceedings EMC Europe Workshop, Paris*, 1–5, 2007.
8. Yucel, A. C., H. Bagci, and E. Michielssen, "An adaptive multi-element probabilistic collocation method for statistical EMC/EMI characterization," *IEEE Trans. Electromag. Compat.*, Vol. 55, No. 6, 1154–1168, Dec. 2013.
9. Li, P. and L. J. Jiang, "Uncertainty quantification for electromagnetic systems using ASGC and DGTD method," *IEEE Trans. Electromag. Compat.*, Vol. 57, No. 4, 754–763, Aug. 2015.
10. Rumsey, V. H., "Reaction concept in electromagnetic theory," *Physical Review*, Vol. 94, No. 6, 1483–1491, 1954.
11. Sy, O., M. van Beurden, B. Michielsen, J. Vaessen, and A. Tijhuis, "Second-order statistics of complex observables in fully stochastic electromagnetic interactions: Applications to EMC," *Radio Science*, Vol. 45, No. RS4004, Jul. 2010.
12. Papoulis, A., *Probability, Random Variables and Stochastic Processes*, McGraw-Hill Companies, Feb. 1991.
13. Soize, C. and R. Ghanem, "Physical systems with random uncertainties: Chaos representations with arbitrary probability measure," *SIAM J. Sci. Comput.*, Vol. 26, No. 2, 395–410, 2005.
14. Debusschere, B. J., H. N. Najm, P. P. Pébay, O. M. Knio, R. G. Ghanem, and O. P. L. Maître, "Numerical challenges in the use of polynomial chaos representations for stochastic processes," *SIAM J. Sci. Comput.*, Vol. 26, No. 2, 698–719, 2005.
15. Haarscher, A., P. De Doncker, and D. Lautru, "Uncertainty propagation and sensitivity analysis in ray-tracing simulations," *Progress In Electromagnetics Research M*, Vol. 21, 149–161, 2011.
16. Sy, O., M. van Beurden, B. Michielsen, and A. Tijhuis, "Semi-intrusive quantification of uncertainties in stochastic electromagnetic interactions: Analysis of a spectral formulation," *Proc. International Conference on Electromagnetics in Advanced Applications, ICEAA 2009*, 2009.
17. Mrozynski, G., V. Schulz, and H. Garbe, "A benchmark catalog for numerical field calculations with respect to EMC problems," *Proc. IEEE International Symposium on Electromagnetic Compatibility*, Vol. 1, 497–502, 1999.
18. Tijhuis, A. and Z. Peng, "Marching-on-in-frequency method for solving integral equations in transient electromagnetic scattering," *IEE Proc. H, Microwaves, Ant. Prop.*, Vol. 138, No. 4, 347–355, Aug. 1991.
19. Champagne II, N. J., J. T. Williams, and D. R. Wilton, "The use of curved segments for numerically modeling thin wire antennas and scatterers," *IEEE Trans. Ant. Prop.*, Vol. 40, No. 6, 682–689, 1992.
20. Tesche, F. M., "Comparison of the transmission line and scattering models for computing the NEMP response of overhead cables," *IEEE Trans. Electromagn. Compat.*, Vol. 34, No. 2, 93–99, 1992.
21. Li, P., Y. Shi, L. J. Jiang, and H. Bagci, "Transient analysis of lumped circuit networks-loaded thin wires by dgttd method," *IEEE Trans. Ant. Prop.*, Vol. 64, No. 6, 2358–2369, Jun. 2016.

22. Rudin, W., *Functional Analysis*, 2nd Edition, ser. International Series in Pure and Applied Mathematics, McGraw-Hill Inc., New York, 1991.
23. Abramowitz, M. and I. A. Stegun, *Handbook of Mathematical Functions with Formulas, Graphs, and Mathematical Tables*, ninth Dover printing, tenth GPO printing ed., Dover, New York, 1964.
24. Walters, R. W., "Towards stochastic fluid mechanics via polynomial chaos," *41st AIAA Aerospace Sciences Meeting and Exhibit*, Vol. AIAA-2003-0413, 2003.
25. Eadie, W. T., D. Drijard, and F. E. James, *Statistical Methods in Experimental Physics*, North-Holland Pub. Co., 1971.
26. Gerstner, T. and M. Griebel, "Numerical integration using sparse grids," *Numerical Algorithms*, Vol. 18, No. 3, 209–232, 1998.
27. Golub, G. and C. Van Loan, *Matrix Computations*, ser. J. Hopkins Studies Mathematical Sciences, Johns Hopkins University Press, 1996.
28. Xiu, D. and G. E. Karniadakis, "The Wiener-Askey polynomial chaos for stochastic differential equations," *SIAM J. Sci. Comput.*, Vol. 24, No. 2, 2002.
29. Steinberg, B. Z., L. B. Felsen, and E. Heyman, "Phase-space beam summation for time-harmonic radiation from large apertures," *J. Opt. Soc. Am. A*, Vol. 8, No. 1, 41–59, Jan. 1991.